Atmos. Chem. Phys. Discuss., 7, 65–91, 2007
www.atmos-chem-phys-discuss.net/7/65/2007/
© Author(s) 2007. This work is licensed
under a Creative Commons License.

Atmospheric Chemistry and Physics Discussions

Interannual variability of the stratospheric wave driving during northern winter

A. J. Haklander[1,2], **P. C. Siegmund**[3], **and H. M. Kelder**[1,2]

[1]Eindhoven University of Technology (TUE), Department of Applied Physics, P.O. Box 513, 5600 MB Eindhoven, The Netherlands
[2]Royal Netherlands Meteorological Institute (KNMI), Climate and Seismology Department, Climate Observation Division, P.O. Box 201, 3730 AE De Bilt, The Netherlands
[3]Royal Netherlands Meteorological Institute (KNMI), Climate and Seismology Department, Climate and Chemistry Division, P.O. Box 201, 3730 AE De Bilt, The Netherlands

Received: 6 December 2006 – Accepted: 14 December 2006 – Published: 5 January 2007

Correspondence to: A. J. Haklander (haklande@knmi.nl)

Abstract

The strength of the stratospheric wave driving during northern winter is often quantified by the January–February mean poleward eddy heat flux at 100 hPa, averaged over 40°–80° N (or a similar area and period). Despite the dynamical and chemical relevance of the wave driving, the causes for its variability are still not well understood. In this study, 45 years of ERA-40 reanalysis data are used to examine several factors that significantly affect the interannual variability of the wave driving. The total poleward heat flux at 100 hPa is poorly correlated with that in the troposphere, suggesting a decoupling between 100 hPa and the troposphere. However, the individual zonal wave-1 and wave-2 contributions to the wave driving at 100 hPa do exhibit a significant coupling with the troposphere, predominantly due to their stationary components. The stationary wave-1 contribution to the total wave driving significantly depends on the latitude of the stationary wave-1 source in the troposphere. The results suggest that this dependence is associated with the varying ability of stationary wave-1 activity to enter the tropospheric waveguide at mid- to subpolar latitudes. If composites of strong and weak wave-driving years are compared, we find significantly higher refractive index values in the midlatitude stratosphere for the strong composite than for the weak composite. Since wave activity tends to propagate towards higher refractive index values, this could explain part of the interannual variability of the wave driving. Finally, an alternative approach is taken, in which the wave driving anomalies are separated into three parts: one part due to anomalies in the zonal correlation between the eddy temperature and eddy meridional wind, another part due to anomalies in the zonal eddy temperature amplitude, and a third part due to anomalies in the zonal eddy meridional wind amplitude. It is found that year-to-year variability in the zonal correlation between the eddy temperature and the eddy meridional wind is the most dominant factor in explaining the year-to-year variability of the poleward eddy heat flux.

1 Introduction

According to the downward-control principle, the stratospheric residual meridional circulation at any level is controlled by the vertically-integrated zonal force due to breaking Rossby and gravity waves above that level (Haynes et al., 1991). The breaking waves deposit westward angular momentum into the relative and planetary angular momentum 'reservoirs', causing a westward acceleration and a poleward displacement of the air (e.g., Andrews et al., 1987). In the low-frequency limit, the westward acceleration is zero and the meridional circulation is referred to as the Brewer-Dobson circulation (e.g., Shepherd, 2000). The term "downward control" can, however, be somewhat misleading, since it is the wave activity emanating from below that determines the amount of angular momentum deposited aloft.

The zonal-mean upward flux of wave activity is represented by the upward component F_z of the Eliassen-Palm (E-P) flux, which for quasigeostrophic flow is proportional to the zonal-mean poleward eddy heat flux $[v*T*]$, where the square brackets denote the zonal average and the asterisk denotes the deviation thereof (e.g. Andrews *et al.*, 1987; Newman and Nash, 2000). In the lower stratosphere, $[v*T*]$ (and therefore F_z) exhibits a strong, positive correlation with the tendency of total ozone at mid- and high latitudes during northern winter (e.g., Fusco and Salby, 1999; Randel et al., 2002). Also, during late northern winter the midlatitude eddy heat flux in the lower stratosphere is highly and positively correlated with the temperature in early March at high latitudes, and consequently with the strength of the polar vortex (e.g., Newman et al., 2001; Polvani and Waugh, 2004). Both observations can be explained by the wave-induced poleward transport of ozone-rich air from the tropical source and the subsequent adiabatic compression at higher latitudes.

This fundamental link between the poleward eddy heat flux and the dynamics and chemistry of the stratosphere is now well understood and also quantitatively employed as a diagnostic to validate coupled chemistry-climate models (CCMs) (Austin et al., 2003; Eyring et al., 2005). Austin et al. used the $[v*T*]$ field at 100 hPa averaged for

January–February over 40°–80° N, hereafter referred to as H_{100}, as a measure of the total midwinter wave activity that propagates from the troposphere into the stratosphere. They evaluated several CCMs with respect to H_{100}, the polar stratospheric temperatures in early spring, and the (almost linear) relationship between both diagnostics. Since almost all of the planetary wave activity crosses the 100 hPa level between 40°–80° N (Hu and Tung, 2003), H_{100} indeed provides a good measure of the total wave activity propagating into the stratosphere. Several studies have been performed to analyze trends in H_{100} (or a similar diagnostic) over the last decades, and to predict future trends. Hu and Tung (2003) found a significant downward trend over 1979-2002 for $[v*T*]$ at 100 hPa, averaged over 50°–90° N and January to March. Austin et al. (2003) compared future H_{100} trends in a number of enhanced-CO_2 climate simulations, and found for most models a slightly negative trend over the next few decades, although at best of marginal statistical significance. One of the models showed a highly significant positive trend. For a doubled CO_2 climate, Sigmond et al. (2004) computed a significant increase of the Northern Hemisphere (NH) stratospheric residual circulation during winter, corresponding to an increase of the poleward eddy heat flux. These examples illustrate that future predictions of H_{100} are very uncertain. However, in a recent multi-model study by Butchart et al. (2006), increasing greenhouse gas concentrations were found to yield an overall strengthening of the Brewer-Dobson circulation and the associated wave driving, with the strongest trend in NH winter. Butchart et al. conclude that it remains an important future task to identify the causes of the increase in wave driving. Thus, despite the fact that it is widely acknowledged that the stratospheric wave driving has a large impact on the dynamics and chemistry of the stratosphere, the causes for its trends and variability are still not well understood.

In the present study, H_{100} is used as a measure of the total midwinter wave activity that propagates from the troposphere into the stratosphere, following Austin et al. (2003), and Eyring (2005). Our analysis puts the emphasis on the *interannual variability* of H_{100}, in order to obtain a better understanding of the causes of this observed variability, at both the interannual and the decadal timescale. Year-to-year variations in

H_{100} can be attributed to many factors. The strength of the tropospheric wave source is an obvious factor, but also the shape of the source spectrum determines the amount of wave activity that reaches 100 hPa, as is described by the Charney-Drazin criterion (Charney and Drazin, 1961). This criterion states that stationary planetary waves can only propagate upward in a westerly zonal-mean flow that is not too strong. Only the longest waves can propagate through stronger westerlies, which implies that during winter only the longest waves can propagate into the stratosphere. The background zonal-mean flow determines the properties of this low-pass filter, and therefore also affects the interannual variability of H_{100}. The main goal of the present study is to investigate to what extent the year-to-year variability in H_{100} is affected by several factors. The factors that are examined include the strength of the total upward wave activity flux in the troposphere, the shape of the wave activity spectrum, the latitude and height of the wave source, and the refractive properties of the background flow. It is also examined whether the zonal correlation between the meridional wind and the temperature has a significant effect on the interannual variability of H_{100}. Our analysis is based on ERA-40 reanalysis data for the period of 1958-2002.

The structure of the paper is as follows. Section 2 gives a description of the data sources and discusses various ways of decomposing the poleward eddy heat flux. The main results are given in Sect. 3, and a summary and discussion of the results is presented in Sect. 4.

2 Data and method

2.1 Data

We use 6-hourly temperature and horizontal wind fields for 45 years (1958-2002) of ERA-40 reanalysis data (Simmons and Gibson, 2000). ERA-40 is produced by the European Centre for Medium-Range Weather Forecasts (ECMWF). The meteorological fields were retrieved for a lat-lon grid of 2.5° × 2.5° between 0°–90° N, at 23 pressure

levels between 1000 and 1 hPa.

2.2 Linear regression analysis

The total poleward eddy heat flux can be decomposed into the sum of several components, such as the stationary and transient wave components. The impact of each component on the interannual variability of the total heat flux can be evaluated by performing a linear regression analysis. This can be understood as follows. It can easily be shown that if $y \equiv \sum x_i$, then the variance of y equals the sum of the covariances between y and the x_i, i.e., $var(y) = \sum cov(x_i, y)$. Thus, $cov(x_i, y)$ can be interpreted as the contribution of x_i to $var(y)$. If we define $b_i \equiv cov(x_i, y) var^{-1}(y)$, where $\sum b_i = 1$, then b_i is the regression coefficient for the linear least-squares fit given by $\tilde{x}_i = a_i + b_i y$. It should be noted that the correlation coefficient r_i between y and x_i can be large, while the associated value of b_i is small. For this reason, it is useful to consider both b_i and r_i. In the present study, y represents the total heat flux and the x_i represent the various components of the total heat flux (see Sect. 2.3). Hereafter the phrase 'a linear regression of v_1 with v_2 is performed' implies that v_1 is the independent and v_2 is the dependent variable.

2.3 Decompositions of the heat flux

The total poleward eddy heat flux, averaged over space and time, can be decomposed by separating the eddy meridional wind and eddy temperature into a stationary and a transient part. If we denote the temporal average over January and February by an overbar, the deviation thereof by a prime, and the cosine-latitude weighted spatial average between 40°–80° N by angle brackets, we can write H at a certain pressure level as

$$H \equiv < \overline{v * T *} > = < \bar{v} * \bar{T} * > + < \overline{v' * T' *} >, \quad (1)$$

ACPD
7, 65–91, 2007

EGU

where H at 100 hPa was previously denoted by H_{100}. The r.h.s. terms of Eq. (1) thus describe the contribution to H by the stationary and transient eddies, respectively.

In addition to the temporal decomposition in Eq. (1), a spatial decomposition can be made by discriminating between the individual zonal wavenumber components of the heat flux. The zonal wave component of the total eddy heat flux is calculated as the product of the wave components of v and T, v_s and T_s (e.g., Newman and Nash, 2000). This yields

$$H = \sum_{s \geq 1} < \overline{v_s T_s} >, \tag{2}$$

where the subscript s denotes the zonal wave-s component. Combining Eqs. (1) and (2) yields

$$H = \sum_{s \geq 1} < \bar{v}_s \bar{T}_s > + \sum_{s \geq 1} < \overline{v'_s T'_s} >. \tag{3}$$

The impact of these individual stationary and transient wave components on the interannual variability of the total heat flux will be evaluated by a linear regression analysis in the next section.

A different way of decomposing the total eddy heat flux, is by noting that $[v * T*]$ can be expressed as

$$[v * T*] = r_{v,T} \sigma_v \sigma_T, \tag{4}$$

where $r_{v,T}$ is the zonal correlation coefficient, and σ_v and σ_T are the zonal standard deviations of v and T. If v or T would consist of only one wave component, then their wave amplitudes would be given by $\sqrt{2}\sigma_v$ and $\sqrt{2}\sigma_T$, respectively, and $r_{v,T}$ would be equal to $\cos \Delta\varphi$, where $\Delta\varphi$ is the phase difference between the v and the T wave patterns. Therefore, $r_{v,T}$ might be considered as the cosine of the 'effective phase difference' between v and T for the total spectrum of waves, with $\sqrt{2}\sigma_v$ and $\sqrt{2}\sigma_T$ representing the effective v and T amplitudes, respectively. To investigate both the

qualitative and the quantitative effects of year-to-year variations in $r_{v,T}$, σ_v, and σ_T on the interannual variability of H_{100}, we use the following approach (e.g., Siegmund, 1994). First, we rewrite the average of Eq. (4) over 40°–80° N and January–February as follows:

$$H \equiv < \overline{r_{v,T}\sigma_v\sigma_T} > \equiv < \overline{r_{v,T}} >< \overline{\sigma_v} >< \overline{\sigma_T} > + \tilde{E} \equiv \tilde{H} + \tilde{E}, \quad (5)$$

where $\tilde{E}$ denotes the error that is introduced by neglecting the zonal and temporal cross-correlations between $r_{v,T}$, σ_v, and σ_T. The validity of the approximation $H_{100} \approx \tilde{H}_{100}$ will be discussed in Sect. 4. Dropping the angular brackets and the overbars, denoting the 45-year mean by a superscript m and the deviation thereof by a Δ, $\Delta\tilde{H}$ can be linearized as:

$$\Delta\tilde{H} \equiv \Delta\hat{H} + \Delta\hat{E} \equiv \sigma_v^m \sigma_T^m \Delta r_{v,T} + \sigma_T^m r_{v,T}^m \Delta\sigma_v + \sigma_v^m r_{v,T}^m \Delta\sigma_T + \Delta\hat{E}, \quad (6)$$

where $\Delta\hat{E}$ denotes the error that arises from the linearization. If Eqs. (5) and (6) are combined, we obtain

$$\Delta H \equiv \sigma_v^m \sigma_T^m \Delta r_{v,T} + \sigma_T^m r_{v,T}^m \Delta\sigma_v + \sigma_v^m r_{v,T}^m \Delta\sigma_T + \Delta\hat{E} + \Delta\tilde{E}. \quad (7)$$

Eq. (7) will be used to analyze the contribution to the interannual variability of H_{100} by the interannual variabilities of $r_{v,T}$, σ_v, and σ_T.

3 Results

The timeseries of H_{100} is displayed as the thick solid line with filled circles in Fig. 1. H_{100} ranges between 10.5 and 20.6 K m s^{-1}, and the average value of H_{100} is 14.5 ± 0.4 K m s^{-1}. There is a slightly positive 1958-2002 trend in H_{100}, but this trend is far from statistically significant (23.4% confidence level). Statistically significant 20-year or even longer-term 'trends' with > 95% confidence levels of both positive and negative sign can be found in the 45-year timeseries of H_{100}. However, these trends seem to

be an aspect of decadal natural variability, as was also noted by Newman and Nash (2000). If we regard H_{100} as the sum of its zonal wave-s components as expressed by Eq. (2), we find that the s = 1-3 components of H_{100} account for more than 90% of H_{100}. The first three wave components of H_{100} are also shown in Fig. 1. Both the variance and the 45-year average decrease with increasing wavenumber. For the majority of the years in the dataset, variations in H_{100} seem to be dominated by the wave-1 variations, indicated by the line with open circles in Fig. 1. However, during much of the 1960s and the early 1970s, H_{100} follows its wave-2 component quite closely (line with filled squares). A relatively constant factor is that the wave-1 and wave-2 variations tend to be opposite. The correlation coefficient for the wave-1 and wave-2 total timeseries is r = –0.45, which is significant at a 99.8% confidence level. Neither of the s = 1–3 components of H_{100} exhibit a significant trend over 1958-2002.

3.1 Wave contributions to interannual variability of H_{100}

To further examine the interannual variability of H_{100}, we decompose H_{100} into its stationary and transient wave components, as expressed by Eq. (3). Taking H_{100} as the independent variable, the linear regression coefficient b_i for the regression of H_{100} with its stationary or transient wave component represents the relative contribution by that wave component to the total variance of H_{100}, as discussed in Sect. 2. Table 1 shows the regression coefficients and the corresponding correlation coefficients for the total (stationary plus transient), stationary, and transient wave 1-5 components of H_{100}. For timeseries of 45 independent elements, the correlation coefficient r_i is significantly different from zero at a >95%, 99%, or 99.9% confidence level if $|r_i| > 0.29$, 0.38 or 0.47, respectively. The sum of the regression coefficients for the total wave 1-5 contribution to H_{100} is 0.97 ± 0.01, with a corresponding correlation coefficient r_i = 0.997 (not shown). Therefore, wavenumbers 6 and higher can be neglected in the analysis of the interannual variability of H_{100}. In fact, almost all of the interannual variability of H_{100} is due to s = 1–3, with a combined regression coefficient of b_i = 0.94±0.03 and r_i = 0.98. Only retaining s = 1,2 yields b_i = 0.80±0.07 and r_i = 0.88. We can thus state

ACPD
7, 65–91, 2007

EGU

that about 80% of the interannual variability of H_{100} can be attributed to its s = 1,2 components. When analyzing the interannual variability of H_{100}, it is sufficient to only consider wavenumbers s = 1–3, or perhaps even s = 1,2. The bottom row of Table 1 clearly shows that the interannual variability of H_{100} is dominated by the stationary waves, with b_i = 0.69±0.09 and r_i=0.77. However, the correlation coefficient of H_{100} with its transient component is also highly significant at the 99.9% confidence level.

3.2 Vertical coupling

As described in the introduction, H_{100} is proportional to the total wave activity flux emanating from below between 40° N and 80° N at the 100 hPa level. The planetary wave activity that constitutes H_{100} has propagated upward from its tropospheric source, and therefore, it is expected that H_{100} has a significant positive correlation with the poleward eddy heat flux at levels below (and above) 100 hPa. To verify this, we examine the amount of vertical coupling between 100 hPa and other levels. We do this by calculating the vertical profile of the correlation coefficient of H_{100} with $< \overline{v*T*} >_{NH}$, which we define as the NH average of $[\overline{v*T*}]$, at levels from 1000 hPa to 1 hPa. We compute the correlation with $< \overline{v*T*} >_{NH}$, since the wave activity flux contributing to H_{100} may have partially originated from latitudes outside the 40°-80° N band below 100 hPa. Also, part of H_{100} may propagate into latitudes outside the 40°-80° N band above 100 hPa. The correlation profile is shown in Fig. 2. At 100 hPa, H_{100} is highly correlated with $< \overline{v*T*} >_{NH}$ (r = 0.92), suggesting that the 100 hPa wave activity outside the 40°–80° N area is relatively small. This is confirmed by the fact that H_{100} accounts for 90% of the total NH upward wave activity flux at 100 hPa during January–February in the 1958–2002 period. Therefore, to simplify the interpretation of our results, we neglect the 100 hPa upward wave activity flux at latitudes outside the 40°–80° N window. In Fig. 2, we see that the level of maximum correlation between H_{100} and $< \overline{v*T*} >_{NH}$ is found at 70 hPa rather than 100 hPa. Above 70 hPa, the correlation gradually decreases to marginally significant values near the stratopause ~1 hPa. Below 100 hPa,

the correlation coefficient falls off quite rapidly, and is not significant ($|r| < 0.29$) below 250 hPa. Thus, there exists a decoupling between variations in the total upward flux of wave activity in the troposphere (below 250 hPa) and variations at 100 hPa. This decoupling can be understood as follows. Suppose an amount of wave activity propagates upward in the NH at some tropospheric pressure level p during January–February. A fraction α_p of this wave activity is absorbed below 100 hPa, where α_p lies between 0 and 1. Assuming that no wave activity crosses the equator, the remaining fraction of the wave activity (1-α_p) thus reaches the 100-hPa level and contributes to H_{100}. If α_p is less than one and independent of time, then the correlation coefficient between H_{100} and the wave activity flux at pressure level p will be one. On the other hand, if α_p has a large interannual variability, the correlation coefficient will be small.

For a plane and conservative planetary wave, the zonal wavenumber s and the frequency remain constant along its path (or "ray") in the meridional plane (e.g., Karoly and Hoskins, 1982). Therefore, it makes sense to repeat the previous analysis for each individual zonal wave component. To examine the amount of vertical coupling as a function of zonal wavenumber (stationary plus transient), we compute the correlation coefficients of the wave-s component of H_{100} with the (same) wave-s component of $< \overline{v*T*} >_{NH}$ at other levels. We perform this analysis for the individual wavenumbers 1 to 5 and 6+, separately. The results are shown in Fig. 3a. At all levels above 850 hPa, the s = 1 component of $< \overline{v*T*} >_{NH}$ is significantly correlated with the s = 1 component of H_{100}. Closer to the surface, only the s = 2 component of $< \overline{v*T*} >_{NH}$ is significantly correlated with the same wave component of H_{100} (r = 0.64 at 1000 hPa). Note that the wave-2 correlation reaches a minimum at 400 hPa (r = 0.39) but that the correlation coefficients for s = 2 are statistically significant at all levels. For waves with s> 2, the correlation coefficients generally only exceed the 95% significance level between 300 hPa and 20 hPa. Thus, the lack of correlation we saw in Fig. 2 between the total upward flux of wave activity in the troposphere (below 250 hPa) and that at 100 hPa is also observed for the s > 2 flux components, but not for s = 1,2. This result implies that a significant part of the interannual variability in the s = 1,2 components of

H_{100} is due to year-to-year variations in the strength of the s = 1,2 wave source in the troposphere.

We have just shown that the separate s = 1,2 components of H_{100}, to which about 80% of the interannual variability of H_{100} can be attributed, are significantly correlated with the separate s = 1,2 components of $< \overline{v*T*} >_{NH}$ in the troposphere. But to what extent can the interannual variability of the *total* H_{100} be attributed to year-to-year variations in the separate s = 1 and s = 2 components (or higher) of $< \overline{v*T*} >_{NH}$ in the troposphere? To answer this question, we examine the correlation of H_{100} (i.e., the sum of all wave components) with the separate wave components of $< \overline{v*T*} >_{NH}$. The results are shown in Fig. 3b, where the wavenumber of the pressure-dependent $< \overline{v*T*} >_{NH}$ component is given along the horizontal axis. At levels below 200 hPa, the s = 1,2 components of $< \overline{v*T*} >_{NH}$ are not significantly correlated with H_{100}. In fact, below 300 hPa, none of the wave components is. However, in the upper stratosphere, the $s > 2$ components of $< \overline{v*T*} >_{NH}$ exhibit a remarkably strong correlation with H_{100}. It is interesting to compare Figs. 3a and 3b. We observe in Fig. 3a that the wave-4 component of $< \overline{v*T*} >_{NH}$ in the upper stratosphere is very poorly correlated with the wave-4 component of H_{100}. However, Fig. 3b shows that the correlation coefficient with the *total* H_{100} is extremely significant for the wave-4 component of $< \overline{v*T*} >_{NH}$ in the upper stratosphere (r = 0.63 at 2 hPa). Another feature in Fig. 3b is, that the zonal wavenumber which has the strongest correlation with H_{100} increases with increasing height above 100 hPa. The pattern thus takes the shape of an energy cascade from lower to higher wavenumbers, as long planetary waves propagate upward and eventually break up into shorter waves before they dissipate.

3.3 Correlation patterns in the meridional plane

Thusfar, we have only considered averages over 40°–80° N and averages over the entire Northern Hemisphere. In the previous subsection we mentioned that α_p also

ACPD
7, 65–91, 2007

EGU

depends on the latitude at which the waves propagate upward. Therefore, we next examine where the *zonal-mean* upward wave-activity flux, which is proportional to $[\overline{v*T*}]$, is significantly correlated with H_{100}. The latitude- and pressure-dependent correlation coefficient of H_{100} with $[\overline{v*T*}]$ is shown in Fig. 4a. The maximum correlation occurs at 100 hPa and 62.5° N ($r = 0.87$). The decoupling between the total upward wave-activity flux at 100 hPa and that in the troposphere (Fig. 2) is also visible in Fig. 4a: H_{100} is not significantly correlated with $[\overline{v*T*}]$ in the lower and middle troposphere. In the stratosphere, the latitude of maximum correlation shifts equatorward with height indicating the equatorward refraction of planetary-wave activity. We previously saw that the s = 1,2 components of H_{100} significantly correlate with the same wave-s components of $<\overline{v*T*}>_{NH}$ in the troposphere. Fig. 4b shows that the wave-1 component of H_{100} is significantly correlated with the wave-1 component of $[\overline{v*T*}]$ in the troposphere, between about 40° N and 60° N. Note that the meridionally confined correlation maximum in the troposphere tilts poleward with height. A possible explanation for this correlation maximum would be the presence of a waveguide, through which the wave-1 activity is ducted to 100 hPa (e.g., Karoly and Hoskins, 1982). Since a waveguide can be identified as a ridge in the refractive index field, we verify this by computing the climatological January–February pattern of the refractive index squared for s = 1, which is shown in Fig. 5a. We see that the refractive index indeed has a ridge in the mid-latitude troposphere, and its axis tilts poleward with height. This suggests that the tropospheric correlation maximum in Fig. 4b may be regarded as the signature of a tropospheric wave guide. To illustrate how the upper troposphere and lower stratosphere act as a low-pass filter for planetary wave activity from below, we show the refractive index field for s = 3 in Fig. 5b. A mid-latitude vertical layer with negative values in the lower stratosphere emerges, of which the vertical extent increases with increasing wavenumber (not shown). In contrast with Fig. 4a, equatorward refraction of wave-1 activity in the stratosphere is not evident from Fig. 4b. For wavenumber 2 (Fig. 4c), a connection with the (lower) troposphere is found that is similar to that of wavenumber 1. A marked

ACPD
7, 65–91, 2007

difference between Figs. 4c and 4b is, that the area of maximum correlation in the troposphere is found at higher latitudes (55–75° N) in Fig. 4c, with a distinct maximum (r = 0.60) at 1000 hPa. For wavenumber 2, the latitude of maximum correlation shifts equatorward with height above 100 hPa, like in Fig. 4a. For the wave-3 contribution to the heat flux, the link with the troposphere is absent and the area with significant correlation coefficients is much more confined (not shown). A further decomposition into stationary and transient wave components (Figs. 4d-i) reveals that the link with the (lower) troposphere is only statistically significant for the *stationary* part of the wave-1 and wave-2 contributions. The tropospheric meridional dipole structure in the stationary wave-1 correlation map (Fig. 4e) implies that the stationary wave-1 component of H_{100} is sensitive to the latitude of the tropospheric wave-1 source. If the source is located too far south, less wave activity is able to enter the mid-latitude waveguide and contribute to H_{100}.

3.4 Refractive index

As shown in Figs. 3 and 4, the s = 1,2 components of H_{100} are significantly correlated with the s = 1,2 components of $< \overline{v*T*} >_{NH}$ in the troposphere. This implies that the interannual variability of H_{100} is not only determined by wave refraction and absorption but also by the variability of the upward wave activity flux in the troposphere. However, the correlation is not perfect, and the interannual variability of the refractive index square pattern ($a^2 n_s^2$) likely also plays a significant role. To examine this, we calculate the difference map for $a^2 n_s^2$ between the years with high H_{100} and the years with low H_{100}. Since the wavenumber-dependent part of the refractive index square is time independent, the difference map is identical for all s (e.g., Andrews et al., 1987). As a threshold, we select the years where $|\Delta H_{100}|$ exceeds one standard deviation, which is indicated by the two straight dotted lines in Fig. 1. For the 1958–2002 period, this yields 8 'high-H_{100}' winters for which H_{100} was greater than $+\sigma$, and 11 'low-H_{100}' winters with a deviation of less than $-\sigma$. The high-H_{100} minus low-H_{100} difference map for $a^2 n_s^2$ is

shown in Fig. 6. In the mid-latitude stratosphere, we find significantly higher indices of refraction in high-H_{100} winters than in low-H_{100} winters. No significant differences are found below 100 hPa. Since wave activity is refracted toward increased values of $a^2 n_s^2$, this implies that more wave activity tends to be directed from the troposphere towards the mid-latitude stratosphere in high-H_{100} winters than in low-H_{100} winters.

3.5 An alternative analysis of the interannual variability of H_{100}

In Sect. 2.3, we mentioned an alternative way of decomposing H_{100}, by noting that $[v*T*]$ equals the product of $r_{v,T}$ with σ_v and σ_T (Eq. 4). Subsequently, we assumed in Eq. 5 that H_{100} can be approximated by $\tilde{H}_{100}$. To examine the accuracy of this approximation, we first compare the 45-year averages of both H_{100} and $\tilde{H}_{100}$. This yields 14.5±0.4 K m s^{-1} and 13.7 ± 0.3 K m s^{-1}, respectively, which is not a significant difference (< 90% confidence level). To see if $\tilde{H}_{100}$ and H_{100} also have comparable interannual variability, we performed a linear regression of H_{100} with $\tilde{H}_{100}$. The regression yields a high correlation coefficient (r=0.90) and a regression coefficient b = 0.73±0.05. We conclude that $\tilde{H}_{100}$ is indeed a useful approximation of H_{100}. We next linearize the deviation of $\tilde{H}_{100}$ from its 1958–2002 mean as $\Delta\hat{H}_{100}$ (Eq. 6). The error $\Delta\hat{E}_{100}$ that arises from the linearization in Eq. (6) is remarkably small: a linear regression of $\Delta\tilde{H}_{100}$ with $\Delta\hat{H}_{100}$ yields b = 0.98±0.03 and r=0.98. The difference between ΔH_{100} and $\Delta\hat{H}_{100}$ in Eq. (7) thus primarily results from $\Delta\tilde{E}_{100}$. We can use Eq. (7) to analyze the sensitivity of H_{100} to the year-to-year variations in the effective phase difference $< \overline{r_{v,T}} >$, as well as to the interannual variability of the effective amplitudes $< \overline{\sigma_v} >$ and $< \overline{\sigma_T} >$. The regression and correlation coefficients of the linear regression analysis of H_{100} with the first three terms on the r.h.s. of Eq. (7) at 100 hPa are given in Table 2. The results show that the interannual variability of H_{100} is more sensitive to the $< \overline{r_{v,T}} >$ than to $< \overline{\sigma_v} >$ and $< \overline{\sigma_T} >$. Therefore, a significant part of the year-to-year variability in H_{100} is not determined by variability in the amplitude of the waves but by variability in the efficiency of the poleward heat transport, as represented by $< \overline{r_{v,T}} >$.

ACPD
7, 65–91, 2007

EGU

We also note that the variability in $< \overline{\sigma_v} >$ affects H_{100} more strongly than the variability in $< \overline{\sigma_T} >$.

4 Summary and conclusions

We have studied the interannual variability of the stratospheric wave driving during NH winter, as quantified by H_{100}, being the January–February mean of the 40°–80° N average of the total poleward heat flux at 100 hPa. For our analysis, we used 45 years (1958–2002) of ERA-40 reanalysis data from ECMWF. The results can be summarized as follows. We have examined the sensitivity of H_{100} to several factors. The first factor is the strength of the total tropospheric wave source. It was found that H_{100} is not significantly correlated with the total upward wave activity flux below 250 hPa. However, both the individual zonal wave-1 and wave-2 components exhibit significant vertical coupling between 100 hPa and lower (as well as higher) levels. About 80% of the interannual variability of H_{100} can be attributed to its s = 1,2 components. However, the interannual variability of H_{100} cannot be attributed to either of these individual wave components of the heat flux in the troposphere. Presumably, this is in part due to the highly significant negative correlation that we found between the s = 1 and s = 2 components of H_{100}. This negative correlation is also observed on an intraseasonal timescale, in association with the leading mode of variability in the NH winter geopotential field, the Northern Annular Mode (NAM) (Hartmann et al., 2000). During high NAM index periods, with a stronger stratospheric polar vortex, the anomalous s = 1 component of the heat flux at 100 hPa was negative, and the anomalous s = 2 component was positive. During low NAM index periods, both anomalies were of opposite sign. Thus, the negative correlation we found on the interannual timescale is also observed on the shorter timescales. The wave-1 contribution to H_{100} was found to depend on the latitude of the wave-1 source. Particularly, if the tropospheric stationary wave-1 source is located near 30° N instead of near 50° N, significantly less wave activity is able to enter the mid-latitude waveguide and contribute to H_{100}.

ACPD
7, 65–91, 2007

Another main result is that the refractive properties of the background flow are significantly correlated with H_{100}, with higher refractive index values in the mid-latitude stratosphere during high-H_{100} winters than during low-H_{100} winters. However, the cause-and-effect relationship is unclear, since the wave driving can be both the cause and the effect of anomalies in the refractive index pattern. Finally, an alternative approach was followed, where the wave driving anomalies were separated into three parts: one part due to anomalies in the zonal correlation between the eddy temperature and eddy meridional wind, another part due to anomalies in the zonal eddy temperature amplitude, and a third part due to anomalies in the zonal eddy meridional wind amplitude. It was found that year-to-year variability in the zonal correlation between the eddy temperature and the eddy meridional wind is the most dominant of the three factors (see abstract).

One could argue that the results depend on the 40°-80°N latitude window that is applied. However, replacing H_{100} with the NH average of $[\overline{v*T*}]$ at 100 hPa yields almost identical results. The present study has focused on the interannual variability of the stratospheric wave driving. We note that the factors that dominate the interannual variability may be different from the factors that dominate the trend. These issues will be subject of our further investigation.

References

Andrews, D. G., J. R. Holton, and C. B. Leovy: Middle atmosphere dynamics, Academic Press, 489 pp., 1987.

Austin, J., Shindell, D., Beagley, S. R., Brühl, C.,Dameris, M., Manzini, E., Nagashima, T., Newman, P., Pawson, S., Pitari, G., Rozanov, E., Schnadt, C., and Shepherd, T. G. : Uncertainties and assessments of chemistry-climate models of the stratosphere, Atmos. Chem. Phys., 3, 1–27, 2003, http://www.atmos-chem-phys.net/3/1/2003/.

Butchart, N., Scaife, A. A., Bourqui, M., de Grandpre, J., Hare, S. H. E., Kettleborough, J., Langematz, U., Manzini, E., Sassi, F., Shibata, K., Shindell, D., and Sigmond, M.: Simula-

tions of antropogenic change in the strength of the Brewer-Dobson circulation, Clim. Dyn., doi: 10.1007/s00382-006-0162-4, 2006.
Charney, J. G. and Drazin, P. G.: Propagation of planetary-scale disturbances from the lower to the upper atmosphere, J. Atmos. Sci., 18, 83–109, 1961.
V. Eyring,Harris, N. R. P. M. Rex, T. G. Shepherd, D. W. Fahey, G. T. Amanatidis, J. Austin, M. P. Chipperfield, M. Dameris, P. M. De F. Forster, A. Gettelman, H. F. Graf, T. Nagashima, P. A. Newman, S. Pawson, M. J. Prather, J. A. Pyle, R. J. Salawitch, B. D. Santer, and D. W. Waugh: A strategy for process-oriented validation of coupled chemistry-climate models, Bull. Am. Meteorol. Soc., 86, 1117–1133, 2005.
Fusco, A. C. and Salby, M. L. : Interannual variations of total ozone and their relationship to variations of planetary wave activity, J. Climate, 12, 1619–1629, 1999.
Hartmann, D. J.,Wallace, J. M., Limpasuvan, V., Thompson, D. W. J., and Holton, J. R.: Can ozone depletion and global warming interact to produce rapid climate change?, PNAS, 97, 1412–1417, 2000.
Haynes, P. H., Marks, C. J., McIntyre, M. E., Shepherd T. G., and Shine, K. P.: On the "downward control" of extratropical diabatic circulations by eddy-induced mean zonal forces, J. Atmos. Sci., 48, 651–678, 1991.
Hu, Y. and Tung, K. K.: Possible ozone-induced long-term changes in planetary wave activity in late winter, J. Climate, 16, 3027–3038, 2003.
Karoly, D. and Hoskins, B. J.: Three-dimensional propagation of planetary waves, J. Meteor. Soc. Japan, 60, 109–123, 1982.
Newman, P. A., and Nash, E. R.: Quantifying wave driving of the stratosphere, J. Geophys. Res., 105, 12 485–12 497, 2000.
Newman, P. A., Nash, E. R. and Rosenfield, J. E.: What controls the temperature of the Arctic stratosphere during the spring?, J. Geophys. Res., 106(D17), 19 999–20 010, 2001.
Polvani, L. M. and Waugh, D. W. : Upward wave activity flux as precursor to extreme stratospheric events and subsequent anomalous surface weather regimes, J. Climate, 17, 3548–3554, 2004.
Randel, W. J., Wu, F., and Stolarski, R. : Changes in column ozone correlated with the stratospheric EP flux, J. Meteorol. Soc. Japan, 80, 849–862, 2002.
Shepherd, T. G.: The middle atmosphere, J. Atmos. Sol.-Terr. Phys., 62, 1587–1601, 2000.
Siegmund P. C.: The generation of available potential energy: a comparison of results from a general circulation model with observations, Clim. Dyn., 11, 129–140, 1995.

Sigmond, M., Siegmund, P. C., Manzini, E., and Kelder, H. : A simulation of the separate climate effects of middle atmospheric and tropospheric CO_2 doubling, J. Climate, 17(12), 2352–2367, 2004.

Simmons, A. J. and Gibson, J. K. : The ERA-40 project plan, ERA-40 Proj. Rep. Ser. 1, 63 pp., European Centre for Medium-Range Weather Forecasts, Reading, UK, 2000.

Table 1. Linear regression coefficients ± their standard error, and correlation coefficients for the linear regression of H_{100} with its total, stationary and transient s=1–5 components. The linear regression is performed over 1958–2002.

s	Regr. coeff. (b_i)			Corr. coeff. (r_i)		
	Tot ± σ	**Stat** ± σ	**Tran** ± σ	**Tot**	**Stat**	**Tran**
1	0.56 ± 0.11	0.48 ± 0.14	0.08 ± 0.08	0.60	0.46	0.16
2	0.24 ± 0.11	0.15 ± 0.10	0.09 ± 0.05	0.31	0.21	0.27
3	0.15 ± 0.05	0.07 ± 0.05	0.07 ± 0.03	0.39	0.21	0.33
4	0.00 ± 0.02	–0.01 ± 0.01	0.02 ± 0.02	0.03	–0.13	0.12
5	0.02 ± 0.01	0.01 ± 0.00	0.01 ± 0.01	0.22	0.29	0.12
all	1	0.69 ± 0.09	0.31 ± 0.09	1	0.77	0.47

Table 2. Linear regression of H_{100} with $\sigma_v^m \sigma_T^m \Delta r_{v,T}$, $\sigma_T^m r_{v,T}^m \Delta\sigma_v$, and $\sigma_v^m r_{v,T}^m \Delta\sigma_T$ at 100 hPa. The linear regression is performed over 1958–2002. The 1958–2002 averages and standard deviations are for $< \overline{r_{v,T}} >$, $< \overline{\sigma_v} >$, and $< \overline{\sigma_T} >$, respectively.

	Regression coefficient	Corr. coeffient	1958–2002 average	1958–2002 stdev
$\sigma_v^m \sigma_T^m \Delta r_{v,T}$	0.39 ± 0.15	0.38	$r_{v,T}^m$=0.24	0.05
$\sigma_T^m r_{v,T}^m \Delta\sigma_v$	0.25 ± 0.09	0.39	σ_v^m=5.7 m s^{-1}	0.7 m s^{-1}
$\sigma_v^m r_{v,T}^m \Delta\sigma_T$	0.08 ± 0.07	0.16	σ_T^m=10.3 K	1.0 K

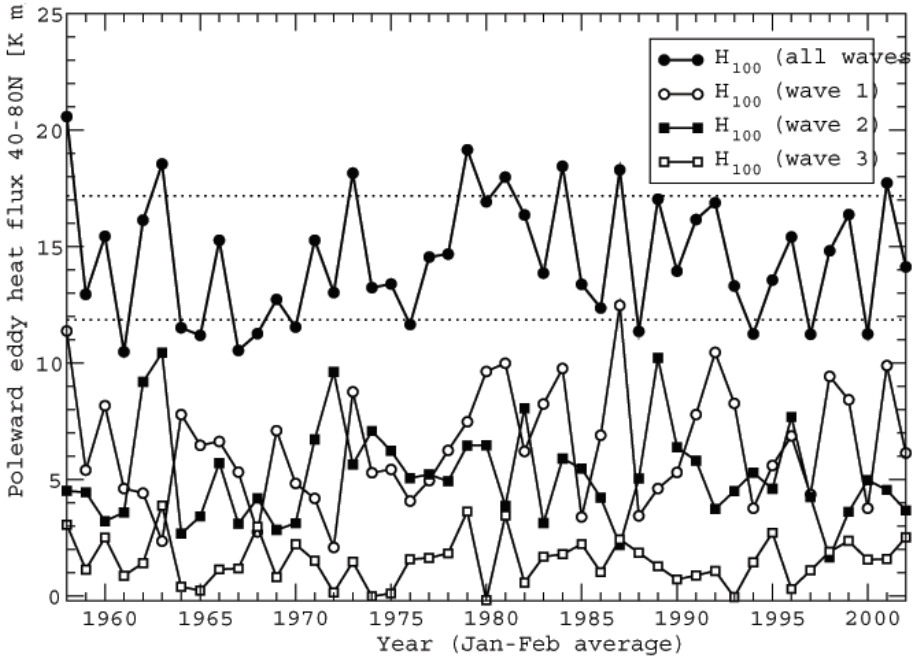

Fig. 1. Poleward eddy heat flux at 100 hPa, averaged over 40°–80° N and January–February, for the years 1958–2002. The sum of all wave contributions H_{100} is shown, as well as the separate wavenumber 1-3 components of H_{100}. The two straight dotted lines mark the standard deviation anomalies of H_{100}.

ACPD
7, 65–91, 2007

EGU

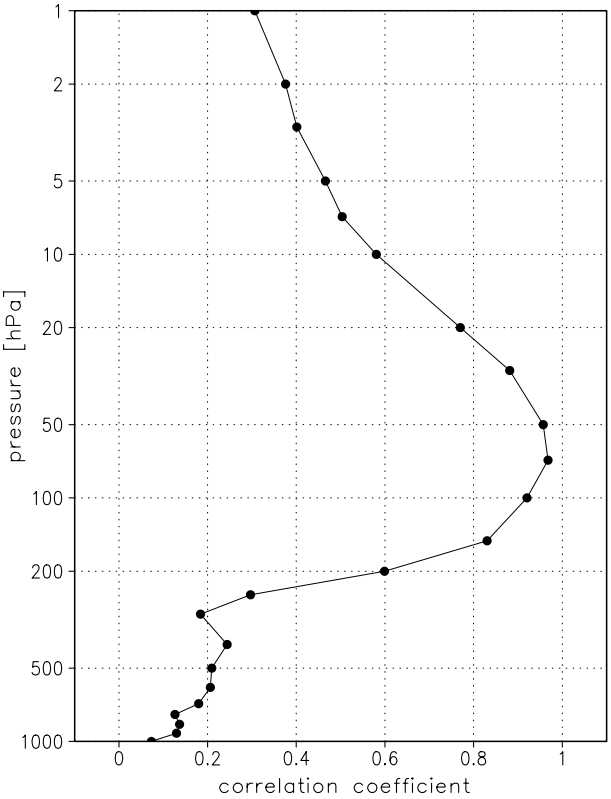

Fig. 2. Correlation coefficients of H_{100} with $< \overline{v * T *} >_{NH}$. Correlation coefficients are calculated over the years 1958–2002.

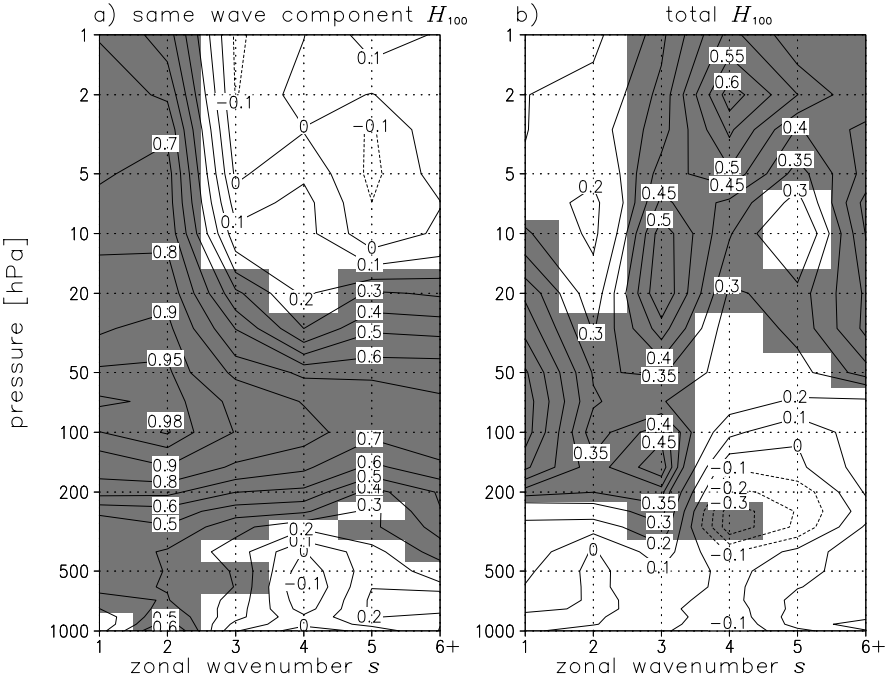

Fig. 3. Correlation coefficients of **a)** the zonal wave-s component of H_{100}, and **b)** H_{100}, with the zonal wave-s component of $< \overline{v*T*} >_{NH}$. Correlation coefficients are calculated over 1958-2002, and the areas with > 95% confidence levels are shaded.

ACPD
7, 65–91, 2007

EGU

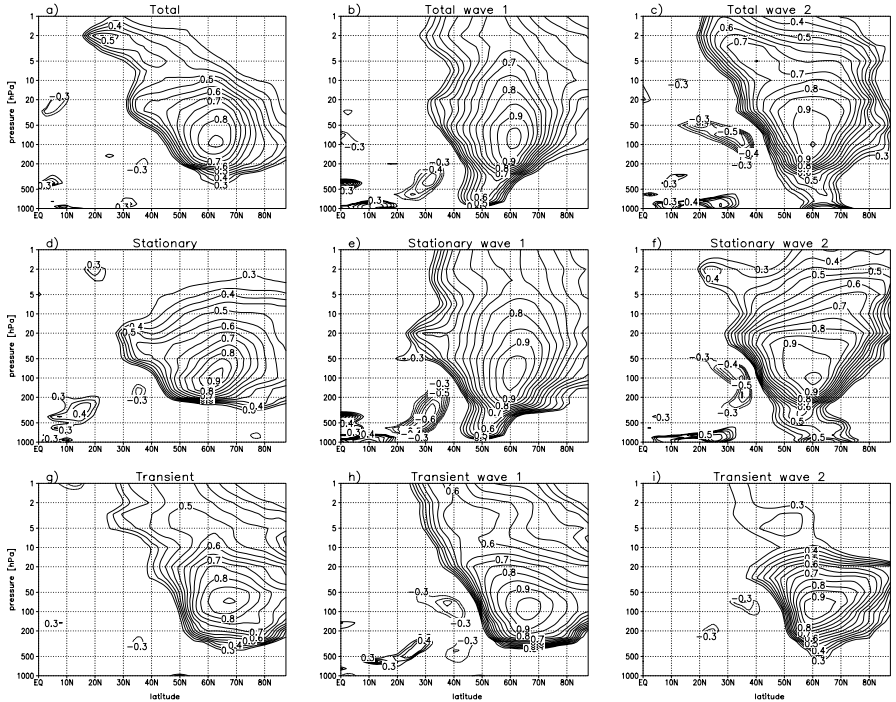

Fig. 4. Correlation coefficient of **(a)** H_{100}, **(b) (c)** the s =1,2 component of H_{100}, **(d)** the stationary component of H_{100}, **(e) (f)** the stationary s = 1,2 component of H_{100} **(g)** the transient component of H_{100},**(h)**, **(i)** the transient s = 1,2 component of H_{100}; with the same latitude- and pressure-dependent wave component of the zonal-mean eddy heat flux averaged over January–February. Correlation coefficients are calculated over 1958–2002, and only the areas with > 95% confidence levels are shown.

ACPD
7, 65–91, 2007

EGU

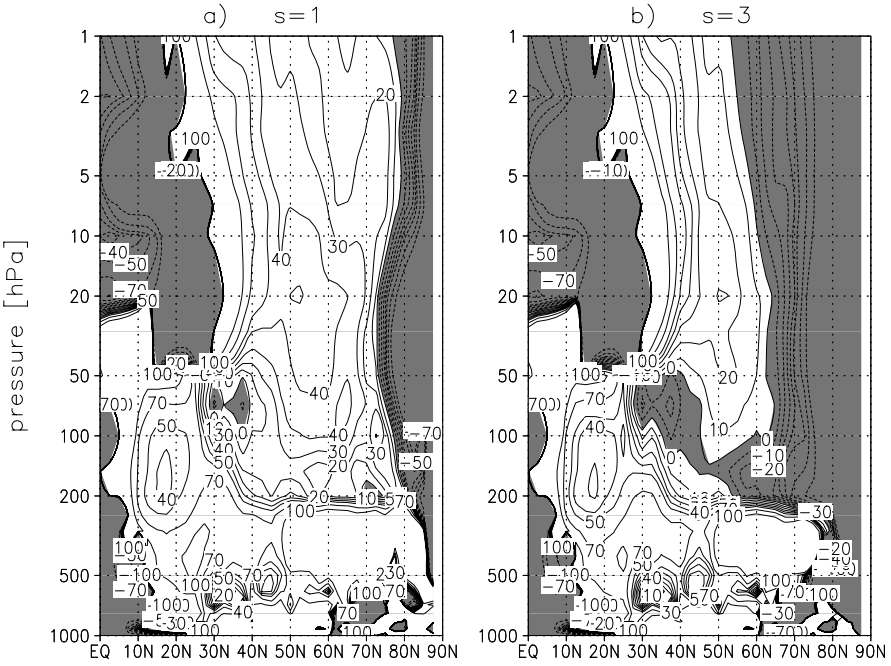

Fig. 5. Refractive index square $a^2 n_s^2$, based on the 45-year average of the zonal-mean zonal wind during January–February, for **(a)** s = 1, and **(b)** s = 3. Areas with negative values have been shaded. Units are m^2.

ACPD
7, 65–91, 2007

EGU

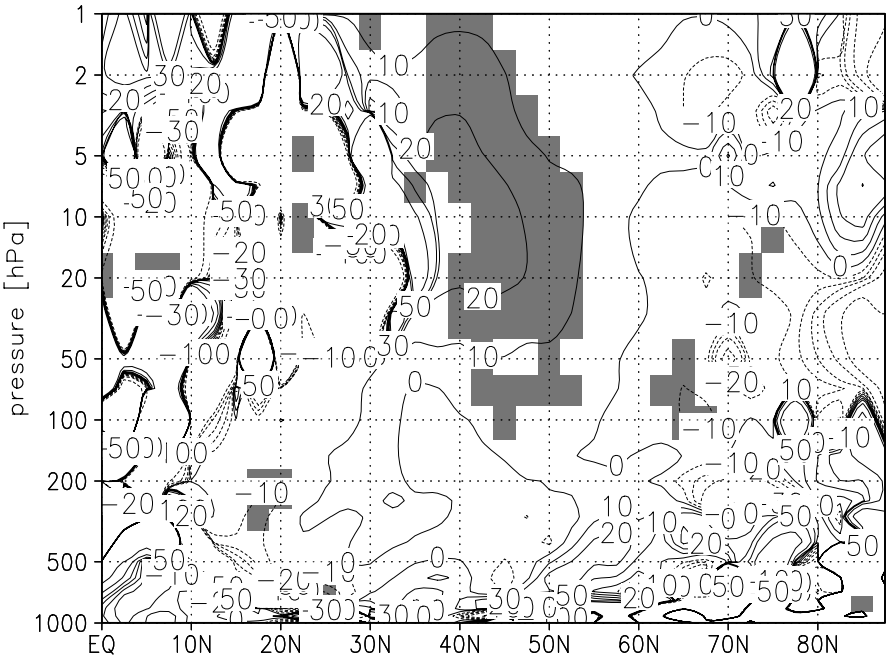

Fig. 6. Difference between 8 high-H_{100} winters ($\Delta H > +1$ stdev) and 11 low-H_{100} winters ($\Delta H < -1$ stdev) in the 1958–2002 period, for the refraction index square a^2n^2 based on the January–February average of $\bar{u}$. The shaded areas denote where the difference is significant above the 95% confidence level. The unit of a^2n^2 is m^2.

ACPD
7, 65–91, 2007

EGU